Post-print of: Ryl J., Burczyk Ł., Zieliński A., Ficek M., Franczak A., Bogdanowicz R., Darowicki K.: Heterogeneous oxidation of highly boron-doped diamond electrodes and its influence on the surface distribution of electrochemical activity. ELECTROCHIMICA ACTA. Vol. 297 (2019), pp. 1018-1027. DOI: 10.1016/j.electacta.2018.12.050

Heterogeneous oxidation of highly boron-doped diamond electrodes and its influence on the surface distribution of electrochemical activity

Jacek Ryl[#,1], Lukasz Burczyk[1,2], Artur Zielinski[1], Mateusz Ficek[3], Artur Franczak[1], Robert Bogdanowicz[3] and Kazimierz Darowicki[1]

[1] Department of Electrochemistry, Corrosion and Materials Engineering, Faculty of Chemistry, Gdansk University of Technology, Narutowicza 11/12, 80-233 Gdansk, Poland

[2] SPZP Corrpol, Elblaska 133a, 80-718 Gdansk, Poland

[3] Department of Metrology and Optoelectronics, Faculty of Electronics, Telecommunication and Informatics, Gdansk University of Technology, Narutowicza 11/12, 80-233 Gdansk, Poland

corresponding author: jacek.ryl@pg.edu.pl

Abstract:

The electrochemical active surface area (EASA) of polycrystalline boron-doped diamond (BDD) electrodes is heterogeneous and can be affected by numerous factors. There is a strong need for proper consideration of BDD heterogeneity in order to improve this material's range of application in electrochemistry. Localized changes in surface termination due to the influence of oxidation agent result in increased surface resistance. The observed behavior of this characteristic feature varies among individual grains, depending on their crystallographic orientation. Still, there is not much information about this key factor in terms of its influence on the electrochemical response of BDD.

In this study we compared two approaches towards BDD surface oxidation, namely: anodic polarization at potentiostatic and potentiodynamic conditions. The surface impedance measurements via Nanoscale Impedance Microscopy (NIM) allowed the confirmation of diversified propensity for the modification of surface termination in BDD. We showed that the NIM studies provide a deep understanding on the electrical characterization and variation of surface resistance in BDD electrodes. In order to evaluate the actual heterogeneity of electrochemical activity distribution, voltammetry, dynamic electrochemical impedance spectroscopy (DEIS) and scanning electrochemical microscopy (SECM) studies were performed. For each investigated electrode, departure from the Randles-Sevcik equation was observed, with its level depending on the surface heterogeneity and oxidation treatment, justifying the standardization of pre-treatment procedure and development of non-standard model for diffusion transport in proximity of BDD electrode.

1. Introduction:

Boron-doped diamond (BDD) is a very attractive material due to its unique semiconducting and electrochemical properties [1,2]. BDD is inert with regard to many chemical reagents and it remains unaffected by high levels of radiation, which makes it suitable for extreme applications. Most BDD electrodes are polycrystalline due to the relative ease at which they can be produced by utilizing microwave plasma (MW PA) or hot filament (HF) CVD [3]. The specific design of the CVD reactor strongly influences the quality and uniformity of the BDD films produced [2]. The growth time and gas composition also affect the grain size and surface roughness. Furthermore, the incorporation of various boron concentrations into the diamond lattice results in the diverse granular film structure and produces non-diamond impurities at the grain boundaries. These factors allow for the controllable induction of specific surface morphology and the presence of sp^2 non-diamond carbon impurities introduced during growth. Thus, the electrical and electrochemical properties of BDD can be controlled [4].

The BDD electrode is known for a wide potential window in aqueous solvents as well as the low background current and reduced fouling [5]. Nevertheless, this unique electrochemical performance depends strongly on the BDD structure, including boron doping concentration, content of sp^2 impurities, and the electrode's surface termination [6]. Moreover, the origin and the influence of both sp^2 and sp^3-bonded carbon in the BDD electrodes is still unclear. The uncontaminated sp^3-bonded carbon surface results in the low catalytic activity toward inner-sphere electron transfer processes, while the sp^2-bonded impurities on the BDD surface enhance the electrocatalytic activity of the electrode [7].

The electrical and optical properties of diamond also depend on its surface termination [8–11]. The hydrogen-terminated boron-doped diamond (HT-BDD) electrodes display a non-polar, hydrophobic surface with negative electron affinity. On the other hand, the oxygen termination of boron-doped diamond (OT-BDD) electrodes leads to a polar, hydrophilic surface with positive electron affinity. By converting the hydrogen termination to oxygen termination, a decrease in the electrical conductivity of BDD surface is induced. The differences in charge transfer resistance between HT- and OT-BDD electrodes have been described in numerous reports [12–16]. Oliveira et al. used EIS to examine the BDD electrodes that had been anodically and cathodically pre-treated [15]. The results obtained by fitting the electrical equivalent circuit (EEC) revealed significant differences, the presented values of charge transfer resistance of OT-BDD were even up to three orders of magnitude higher than those of HT-BDD. A similar tendency was observed in other studies [17,18].

A strong increase in charge transfer resistance is a consequence of the elimination of hydrogen on the BDD surface and the decreased conductivity of BDD. The modified Mott-Schottky relationship after the electrochemical oxidation treatment was described in several reports, where the observed positional shift in the flat band potential suggests a relationship between a decrease in charge transfer and the positional

shift of band edges [13,14]. It is important to note that the Mott-Schottky relationship strongly depends on crystallographic orientation, and thus on the texture of BDD electrode [19].

Hoffmann et al. [20] investigated various electrolyte-stable surface terminations under different electrochemical oxidation treatments. The AFM studies of BDD electrodes with HT-selective nitrophenyl diazonium attached to the surface demonstrated that the electrochemical oxidation can control the fractional hydrogen/oxygen surface termination on a nanoscale. Wilson et al. [21] also studied the spatial variation of electroactivity in the BDD film by using AFM, cathodoluminescence and SECM. Nonuniform boron uptake across the surface was observed, consequently leading to different conductivity in individual grains. This characteristic, complex feature has been linked to the local electrochemical activity of BDD.

The effect of crystal texture on electrochemical properties has been observed by Pleskov et al. [19,22], who reported varying Mott-Schottky behavior of homoepitaxial BDD films grown at the (111), (110) and (100) faces of diamond crystals. The lowest acceptor concentration was present in (100)-oriented faces, while the highest acceptor concentration, in (111)-oriented faces. The reported value of flat-band potential, measured in 2.5 M H_2SO_4, varied between +1.3 and +2.0 V for (110)- and (111)-oriented faces, respectively. It was also found that the kinetics of $[Fe(CN)_6]^{3-/4-}$ oxidation/reduction process varied for different oriented faces.

Recent studies by Ryl et al. [8,23] revealed that the aforementioned fractional surface termination may be a result of the multistage oxidation process, depending not only on the oxidation voltage, but also on the crystallographic orientation, and possibly presence of B-rich active sites [24,25]. Based on the instantaneous impedance studies carried out during anodic polarization, the gradual changes in capacitance dispersion were detected; they occurred at a polarization potential similar to the flat-band potential values for various oriented faces, as previously reported by Pleskov [22]. Such an observation indicates the occurrence of changes within the depletion layer, which is characteristic for the conversion from the hydrogen-terminated to oxygen-terminated surface [13,14]. This conclusion is supported by the modification of capacitance dispersion characteristics measured at the modified BDD electrode. The applied prolonged chemical-assisted mechanical lapping (CAML) pre-treatment led to a significant decrease in the contribution of (111)-oriented faces and the subsequent disappearance of quasi-capacitance peak located at 2.1 V vs Ag|AgCl [26].

The heterogeneous distribution of surface electrical properties resulting from the electrochemical treatment was further reported by using multifrequency nanoscale impedance microscopy (m-NIM), which is a variation of AC signal probing implemented to AFM in contact mode [27]. The studies allowed the confirmation of the gradual variation of local surface resistance under anodic polarization, exceeding 1.5 V vs Ag|AgCl, where a significant increase in the surface area displaying higher resistance, due to oxygen termination, was observed. Based on the NIM, impedance and Mott-Schottky analyses as well as

the EBSD and XRD studies, a conclusion was reached that the propensity for oxidation depends on the crystallographic orientation of particular BDD crystallites. The oxidation propensity sequence was proposed, as follows: (110) > (100) > (111). It is important to point out that both the surface oxidation propensity and boron uptake appear to be dependent on crystallographic orientation, although the relationships do not directly affect each other.

Based on the application of m-NIM, Zielinski et al. [28] successfully confirmed that the fractional modification of hydrogen/oxygen surface occurs not only as a result of electrochemical oxidation, but also due to other treatments, i.e. high-temperature oxidation, atmospheric ageing and, to a lesser extent, chemical and oxygen plasma treatments. However, in each case the oxidation propensity coincides with the crystalline structure of BDD as it most likely depends on crystallographic texture. Unlike XPS or the contact angle analysis, m-NIM enables the determination of local oxidation homogeneity.

The local distribution of more and less conducting areas on the surface of BDD electrode will affect the diffusion field and charge transfer kinetics. This issue is of high importance in many fields, such as when investigating the interface between a BDD electrode and proteins, where the optimization of surface chemistry creates a highly functional biointerface [29], for biosensors, energy harvesting and electroanalytical devices. Furthermore, identifying the relationship between the material structure and electrode performance is crucial for defining the parameters of BDD growth and post-processing technology because the BDD structure can be controlled during the film growth.

The aim of the present study is to assess the influence of the heterogeneous distribution of electric properties on electrochemical characteristics of polycrystalline highly boron-doped diamond electrodes. Conditions of the electrochemical oxidation procedure are often overlooked, while significantly influencing the global electrode response. The unique results obtained by means of NIM and SECM microscopies served to provide insight on local distribution of electric properties due to oxidation. Observed deviations from typical kinetics of flat homogeneous electrodes signify the necessity of non-standard calculation model development but also standardization of the applied pre-treatment procedures [30,31].

2. Experimental

2.1. Boron-Doped Diamond electrodes and modification

The BDD electrodes (attn. 10000 ppm [B]/[C] in plasma) were synthesized in MWPECVD system (SEKI Technotron AX5400S, Japan) on p-type Si wafers as reported elsewhere [32,33]. A 6 h growth period produced microcrystalline diamond of ca. 2 μm in thickness, dominated by (110) and (111) facets, containing also (100)-oriented crystals revealed by morphological investigation [27,34]. In order to obtain H-terminated surface and etch sp^2-C phase impurities, a pre-treatment was applied to the deposited BDD

electrodes. First, metallic impurities were dissolved in a hot aqua regia (HNO_3:HCl/1:3, *v-v*). Next, a hot "piranha" solution (H_2O_2:H_2SO_4/1:3, *v-v*) at 90 °C was used to remove organic impurities. The microwave hydrogen plasma treatment was performed using 1000 W microwave power and 300 sccm of hydrogen gas flow for 10 min. Thus, the BDD surface was made predominantly hydrogen-terminated [35].

The electrochemical oxidation pre-treatment was conducted in 1M H_2SO_4, using two separate approaches, namely: potentiodynamic polarization and potentiostatic polarization. In potentiostatic mode the BDD electrode was subjected polarization at potential ranging between 0.5 V and 2.5 V vs Ag|AgCl, with the electric and electrochemical measurements carried out between polarization steps. This approach allowed to monitor the changes occurring exactly at the same area of the electrode. The duration of each polarization step was equal to 20 min. On the other hand in potentiodynamic approach the electrodes were subjected to linear sweep voltammetry (LSV) initiated at open circuit potential and performed in anodic direction up to previously mentioned potential value. Here, the scan rate was 20 mV/s. The polarization potentials used in this study were chosen accordingly to the multistage surface oxidation theory, based on earlier studies by others [8,27].

2.2. Multifrequency Nanoscale Impedance Microscopy analysis

An AFM Ntegra Prima device manufactured by NT-MDT (Russia) was used to analyze samples. The force at the level of 8.7 μN was maintained during contact measurements. The measurements were taken by using CDTP-NCHR conductive probes, manufactured by Nanosensors. Conductivity was ensured by a boron-doped diamond layer covering probes. As declared by the manufacturer, the contact resistance for the described device type is not more than 3 kΩ on a platinum surface. The geometric dimensions of the probe lever were 125x28x4.2 (LxWxT in μm), while other parameters were as follows: resonance frequency: 508 kHz, spring constant: 130 N/m, radius of tip curvature: 200-300 nm. A set of $Z(\omega_n,x,y)$ impedance maps can be obtained by using the approach previously suggested elsewhere [36]. The impedance maps may be presented in the Bode projection: $|Z(\omega_n,x,y)|$ and $\Delta\phi(\omega_n,x,y)$; or in the Nyquist projection as $Z'(\omega_n,x,y)$ and $Z''(\omega_n,x,y)$. In addition, due to the fact that for each pixel of the topographic image, a spectrum from the frequency range between $\omega_1 \cdots \omega_N$ is obtained, it was possible to apply a fitting procedure on the basis of an appropriate electric equivalent circuit. In the present work the low frequency part of the spectrum was used as the estimate of the overall resistance of the probe-tip system.

2.3. Electrochemical studies

All DC electrochemical measurements, including electrochemical pre-treatments, were carried out by using Gamry Reference 600+ (Gamry Instruments, USA) potentiostat/galvanostat with a three-electrode setup, unless otherwise stated. The exposed electrode surface area was 0.5 cm^2.

The oxidation pre-treatment procedure was monitored by means of Dynamic Electrochemical Impedance Spectroscopy in order to track on-line changes of electric parameters in the time domain. DEIS offers a unique opportunity to record impedance spectra in a very short time through the utilization of multifrequency perturbation signal instead of classic frequency-by-frequency approach as well as the reduction of frequency band to approx. 1 Hz [37]. The details of DEIS experimental approach are presented elsewhere [38–40]. DEIS was successfully used to monitor various non-stationary processes in the field of applied electrochemistry and corrosion [41–48], proving its worth with regard to tracking the subtle changes in surface heterogeneity, resulting in capacitance dispersion and surface distribution of time constants [49–51].

Multifrequency perturbation signal was composed of 32 elementary sinusoids in the frequency range between 7 Hz and 94 kHz, with properly predetermined amplitudes and phase shifts [38]. The resultant perturbation signal amplitude did not exceed 15 mV. DEIS was operated using PXIe-4464 and PXIe-6124 (National Instruments, USA) cards for AC signal generation and acquisition, respectively, closed in PXIe-1073 chassis. The multifrequency signal was superimposed with DC polarization signal by means of a Gamry Reference 600+ device.

Voltammetry measurements were carried out at various polarization scan rates between 10 and 1000 mV/s. The electrolyte was composed of 5mM equimolar mixture of $[Fe(CN)_6]^{3-/4-}$ in 0.5 M Na_2SO_4. In both voltammetry and impedance studies the reference Ag|AgCl electrode was an open silver rod covered with silver chlorides, while Pt mesh served as a counter electrode.

Scanning Electrochemical Microscopy (SECM) was performed by using three-step motor system with a resolution of 1 µm in each direction (Sensolytics, Germany). The system was coupled to an Autolab 302N expanded with dual mode bipotentiostat module. The positioning system was supported by a CCD camera. Commercially available ultramicroelectrodes (UME) made with platinum wire sealed in the glass were used in this study. The diameter of platinum disk was equal to 5 µm, and each probe was polished and rinsed with acetone. The electrolytic solution was composed of 2.5 mM $K_4[Fe(CN)_6]$ and 0.5M Na_2SO_4. The electrolyte was purged with argon prior to the experiment. During all experiments, the potential applied to UME and the BDD sample was +0.4 and 0.0 V versus Ag|AgCl reference electrode, respectively. For this setup, the oxidation of redox species occurred at the electrode tip, while the reduction, at the BDD electrode. The approach curves were plotted with a step that was 5 times smaller than the diameter of the platinum disk part of UME. The SECM maps were recorded with a scanning speed equal to 5 µm s^{-1} and 1 µm step in the x-y plane.

2.4. X-Ray Photoelectron Spectroscopy analysis

High-resolution X-Ray Photoelectron Spectroscopy (XPS) analysis was performed in order to determine the degree of surface modification as a result of various electrochemical pre-treatments. The samples were analyzed by means of an Escalab 250Xi multispectroscope (ThermoFisher Scientific, USA), equipped with a monochromatic Al Kα source. 10 eV pass energy and 650 μm X-ray spot size were set. The spectroscope was calibrated using Cu and Au single crystals. Charge compensation was controlled through low-energy electron and low-energy Ar^+ ion emission by using the flood gun (emission current 150 μA, beam voltage 2.1 V, filament current 3.5 A). The spectral deconvolution was carried out by employing Avantage sorfware (ThermoFisher Scientific, USA).

3. Results and discussion

3.1. Heterogeneous distribution of OT-BDD modification

The Multifrequency Nanoscale Impedance Microscopy technique was used in order to demonstrate the heterogeneous distribution of surface resistance across the polycrystalline BDD electrode. The technique was effectively applied to identify local nanoscale variations in surface resistance, which originated from the selective conversion of HT-BDD to OT-BDD under different oxidation pre-treatments [27,28]. In order to analyze the impedance spectra, an $R_S(CR_P)$ EEC was used. The EEC takes into account local resistance of studied material (spreading resistance), parallel tip/sample contact resistance as well as parasitic capacitance of contact and neighboring part of the probe cantilever. In the standard approach, one assumes stable contact force and resulting constant nano-contact resistance. Therefore, application of the perturbation signal with sufficiently high frequency allows providing impedance maps for local spreading resistance changes. However, according to the literature reports [52] as well as authors‘ observations for semiconductor materials the aforementioned assumption is false and nano-contact resistance may be subject of changes. For this reason, it was decided to analyze the low-frequency spectral range, where the impedance of the capacitor is very high and the overall resistance depends only on nano-contact resistance and studied material resistance. It is assumed that surface resistance corresponds to the sum of these two resistances.

The fitting procedure was carried out using a software based on the Nelder-Mead algorithm [53]. Finally, the sum of series resistance and parallel resistance (R_S+R_P), primarily dependent on the surface resistance, was used to plot the impedance maps, as shown below. The full procedure was described in detail in a previous work [28].

Figs. 1b and 1c present the m-NIM-based impedance maps obtained via the aforementioned approach after the potentiostatic polarization pre-treatment at exemplary potentials of 1.6 and 2.5 V vs Ag|AgCl, respectively. Both these maps were recorded in the same area on the electrode, while the AFM contour micrograph of investigated area is presented at Fig. 1a. The local distribution of measured electric

resistance corresponds to crystalline structure, where the selective oxidation of certain crystallites is clearly visible. It was previously suggested that the oxidation propensity is related to crystallographic orientation, assuming the following oxidation sequence: (110) > (100) > (111) [27]. The higher the voltage during the polarization treatment, the more complete the BDD termination transformation into OT-BDD. Analogous micrographs recorded after potentiodynamic pre-treatment at polarization potentials ranging to 1.6 V and 1.9 V are presented on Fig. 1d and 1e, respectively.

The surface resistance of hydrogen-terminated BDD electrodes is significantly lower than that of oxygen-terminated ones, and it does not exceed the MΩ range (typically, the kΩ range is observed for heavily doped BDD electrodes) [21,27,28,54,55]. Thus, in order to determine the degree of oxidized area using m-NIM, a soft oxidation threshold was set at R_S+R_P = 10 MΩ. If the locally found value of surface resistance exceeds the threshold value, the area will be considered as oxidized. The results of surface oxidation obtained by using the aforementioned approach are visualized in Fig. 1f. For HT-BDD, less than 5% of the electrode surface area displayed the surface resistance values above 10 MΩ. The highest level of surface heterogeneity was observed as a result of mild potentiostatic polarization at 1.6 V vs Ag|AgCl (Fig. 1b), where the estimated oxidized area was around 60 %. A higher polarization voltage led to more electrically homogeneous (~88 % oxidized) surface area with significantly higher surface resistance, falling in the GΩ range. On the other hand, BDD electrodes subjected to potentiodynamic polarization pre-treatment are characterized with significantly higher value of surface resistance, denouncing higher level of surface oxidation. Furthermore, polarization scan reaching 1.6 V leads to higher surface homogeneity, exceeding 95 % of surface oxidation.

The high-resolution XPS analysis of BDD electrodes exposed to both types of pre-treatment confirmed electrode's gradual oxidation under applied conditions. With increasing anodic polarization potential the oxidation was more complete, as predicted on the basis of m-NIM studies. The recorded *C1s* spectra are presented in Fig. 2. The obtained spectra were deconvoluted to identify the shares of surface chemical states, and then subjected to detailed analysis. The results of spectral deconvolution are presented in Table 1. Analogous XPS studies for both: potentiodynamically [8] and potentiostatically [27] polarized BDD electrodes are presented elsewhere.

In *C1s* region, two major deconvolution components were located at 284.3 and 285.0 eV, which have been attributed to sp^3-C CH species on the hydrogenated diamond surface (C-C_H) and polyhydride CH species adsorbed to non-hydrogenated BDD surface (C-C_O), respectively. These values are in good agreement with heavily boron-doped (2×10^{21} cm^{-3}) BDD electrodes with dominant (110) and (111) texture components, as used in this study [56,57]. The component characteristics for oxygen terminated surface were recorded at higher binding energies, i.e. the hydroxyl species (C-OH) at 285.9 eV, and a wide tail of carbonyl and carboxyl species (C=O) shifted from +3.2 to +4.7 eV vs C-C_H peak. A small sp^2-C

contribution was noted at 283.3 eV, typically not exceeding 2 at.%, which is a sign of the onset of material failure under the oxidation treatment. Importantly, the peak locations were in perfect agreement with those reported in similar XPS studies on BDD electrodes [8,24,26,58–60].

Because the C-C_O, C-OH and C=O components are primarily related to the modified OT-BDD surface, it is possible to roughly estimate the share of oxidized surface based on the ratio of *C1s* peak components. Electrochemical oxidation is negligible for the polarization voltage of 0.5 V, while it significantly increases for the values exceeding 1.6 V vs Ag|AgCl. The most dominant oxidized forms were the hydroxyl species, but interestingly enough, the amount of carbonyl and carboxyl species highly depended on the polarization voltage. It should also be noted that in terms of chemistry proposed pre-treatment approaches does not differ significantly. The varying efficiency of the applied oxidation pre-treatments is clearly visible, where potentiodynamic polarization appears to be more efficient producing significantly higher amount of hydroxyl groups.

While the present study is focused on the electrochemical oxidation, it has been observed that other types of surface oxidation mechanisms may also introduce heterogeneity into the termination transition of polycrystalline BDD electrodes. A similar observation was made in reference to chemical oxidation in boiling concentrated H_2SO_4, high-temperature exposure in air at 600 °C, oxygen plasma treatment with UV radiation as well as a prolonged exposure to the atmospheric air [28]. The local areas of varying surface resistance correspond to the crystalline structure of BDD, while the level of oxidation efficiency differs between the applied procedures.

The oxidation rate of BDD electrodes can also be monitored on-line using DEIS throughout the electrochemical oxidation process. In the past, DEIS was successfully used to study the surface modification of BDD electrodes during the experiments carried out under potentiodynamic conditions revealing its multistage character [8,23,26], therefore within this work we focus on the impedance effect obtained during potentiostatic polarization.

The application of impedance approach requires the use of EEC for data analysis. A Randles circuit or its derivative has been employed in the majority of BDD studies; it is typically modified through the substitution of capacitance with a constant phase element (CPE) to account for the heterogeneity of the electrode material [8,15,61,62]. Similarly, a simple EEC is best suited to represent the DEIS spectra due to its restriction in the measured signal frequency range. Here, parallel resistance R_{CT} describes resultant charge-transfer resistance through the electrode surface, while CPE represents the quasi-capacitance of the double layer.

BDD is a heterogeneous material, where local distribution of electric properties depends, *inter alia*, on boron distribution, sp^2-carbon contamination, grain boundaries, and crystallographic orientation [6,8,61]. The local surface oxidation and transformation of HT- into OT-BDD may also contribute to the increase

in surface heterogeneity. The surface electrochemical heterogeneity manifests itself in capacitance dispersion, which can be effectively tracked through CPE. The impedance of CPE is defined by the following equation: $Z_{CPE} = 1/Q(j\omega)^n$.

In Fig. 3a, the normalized changes in BDD's charge transfer resistance during the oxidation experiment are shown, as obtained by means of the above discussed EEC. The normalization procedure was essential since the measurements have been carried out under different potentiostatic polarization conditions, while the R_{CT} value depends, to a large extent, on the polarization resistance. The direct result of the deep anodic polarization pre-treatment was an increase in charge transfer resistance that has eventually reached two orders of magnitude. It has been widely reported that the conversion from HT- into OT-BDD surface is reflected by significantly higher R_{CT} values, while the degree of changes is a good indicator of oxidation efficiency [12–16], similar as in the case of surface resistance changes observed through m-NIM.

The H-termination shows p-type surface conductive channel that contribute significantly to the decrease of charge-transfer resistance [13]. Once the BDD surface starts to pre-dominantly oxygen terminated the increase of R_{CT} is registered [15]. Secondly, the effect of anodic treatment on the bulk resistance R_S is much more complex and direct phenomena standing behind that effect was not revealed up to date. It could be attributed to the different factors like removal of non-diamond phases [63], abstraction of un-saturated CH groups [64] or oxidation of boron cluster to B_2O_3 [4,65,66].

Furthermore, higher anodic polarization potential results in a more dynamic surface modification and bigger increase in the R_{CT} value. It is important to note that shallow polarization at 0.5 V vs Ag|AgCl has a negligible effect on the electrode resistance. According to previous studies, such polarization potential is not sufficient to oxidize the terminal bonds as the process is initiated at around 1.5 V in 1M H_2SO_4 [8].

The surface distribution model of time constants was utilized to estimate the effective value of capacitance C_{eff} [67] which, in turn, enabled the estimation of the double layer capacitance based on the CPE results. Afterwards, the C_{eff} values were normalized as in the case of R_{CT} values, and presented in Fig. 3b. It can be concluded that the anodic polarization depth led to a decrease in the effective capacitance value, although the change was much smaller and did not exceed 5-15%. Again, the changes in capacitance for the sample polarized at 0.5 V vs Ag|AgCl (potential insufficient for the OT-BDD transition) were negligible. The initial values of R_{CT}^0 and C_{eff}^0 are summarized in Table 2. The lowest R_{CT} values at the highest polarization potential 2.5 V is a result of oxygen evolution process and removal of the carbon contamination from the BDD electrode surface [15]. The obtained values are in good agreement with those reported in previous potentiodynamic studies employing DEIS [8].

The CPE exponent n is a direct measure of the electrode heterogeneity because for n = 1, Z_{CPE} describes the impedance of a capacitor, and Q = C. Therefore, a decrease in the CPE exponent n marks an increase in electrode heterogeneity. Such situation is illustrated in Fig. 3c, where the potentiostatic polarization at

1.6 V and 2.5 V vs Ag|AgCl was sufficient to initiate oxidation and the modification of surface termination with hydroxyl, carbonyl and/or carboxyl functional groups [8,15,59]. On the other hand, the polarization at 0.5 V, which is insufficient for the surface modification, did not negatively influence the surface homogeneity of BDD. The fluctuation of this parameter changed over time, in particular for the sample polarized at 2.5 V. This finding may be associated with the high dynamics of the oxidation process at deep anodic potentials and short-term changes in geometric surface area due to ongoing oxygen evolution.

3.2. The influence of termination heterogeneity on the electrochemical response

Regardless of the applied oxidation procedure, the conversion of BDD surface from hydrogen-terminated to oxidized is a gradual process, which not only depends on the applied oxidation energy and time, but also on the oxidation method [28]. Since HT- and OT-BDD surfaces exhibit significantly different electrical and electrochemical characteristics, it is important to determine to what extent the heterogeneous distribution of surface termination influences the electrochemical behavior of BDD electrode, if at all.

The scanning electrochemical microscopy (SECM) measurements were carried out to investigate the local variations in the electrochemical activity of oxidized BDD electrodes via potentiostatic and potentiodynamic mode. Selected approach curves for electrochemically oxidized BDD are presented in Fig. 4. For all measurements on HT-BDD electrodes, the approach curves displayed a positive feedback. The same behavior was observed in the case of BDD electrode oxidized at a potentials not exceeding 1.5 V vs Ag|AgCl. The situation started to change close to the potential value at which the transformation of HT-BDD into OT-BDD occurs. For the anodic oxidation exceeding 1.6 V (for both potentiostatic and potentiodynamic pre-treatments), the results were characterized by increasingly higher negative feedback. Such a tendency of approach curves unambiguously demonstrate that the electron transfer was increasingly lower for each subsequent oxidation step [68,69]. However, it should be noted that during potentiostatic polarization some investigated electrodes treated at 1.6 V revealed positive feedback. This phenomenon indicates that not all electrodes were affected to the same extent under the same experimental conditions. The above-mentioned aspect was not observed at higher polarization potentials; all curves for the analyzed BDD electrodes were characterized by negative feedback. Moreover the shape of approach curves was quite independent of the polarization mode.

Figure 5 show the effect of electrochemical pre-treatment on the local distribution of the kinetics of $[Fe(CN)_6]^{4-}$ oxidation, as assessed via SECM. In order to compare different samples and experimental conditions, the Z-axis in all graphs were normalized with regard to the range of color scale and the minimum value. Tip current displayed on each map was negatively shifted to the position where the lowest recorded value equaled zero (i_T*). Such adjustment helped to identify the regions where the

chemical reactivity of the sample surface was more or less homogeneous. The relative current values are less important than the changes in relative current between the samples because the tip current strongly depends on the working distance. Furthermore, in this case each map was obtained at the exact same place.

The obtained SECM micrographs allowed to observe changes in the surface distribution of electrode areas displaying various electrochemical reactivity. The lowest spread of the measured redox currents was observed in the case of BDD electrode polarized at 0.5 V vs Ag|AgCl, where the voltage was insufficient for the HT- to OT-BDD transformation. The highest heterogeneity of chemical reactivity was found for the sample potentiostatically polarized at 1.6 V. The aforementioned polarization depth was reported as sufficient for the oxidation of (110)-oriented planes, having smaller effect on other major planes [27].

Similar, in the case of potentiodynamically polarized BDD electrodes the highest tip current spread was observed at 1.6 V, with two differences: (i) surface heterogeneity was significantly lower and (ii) areas owing different electrochemical reactivity are more localized in this case. This is in good agreement with m-NIM results, where singular small low surface resistance areas (refer to Fig. 1d) could indicate altered distribution of the diffusion layers, not highly overlapping in this particular case [70]. Thus, the application of statistical tools for evaluating the level of heterogeneity seemed very promising.

For each analyzed electrode, the heterogeneity of electrochemical activity on the BDD electrode surface can be tracked using arithmetical mean deviation of the assessed SECM profile (R_a), as presented in Table 3. It is noteworthy that the parameter R_a can provide information about the electrochemical active surface area (EASA) heterogeneity regardless of the average value of charge transfer resistance. Based on the comparison of R_a values, it was found that the sample polarized at 1.6 V vs Ag|AgCl reached the highest level of heterogeneity, which significantly decreased with anodic polarization depth. Thus, it is possible to postulate that the heterogeneous distribution of EASA corroborates (and depends on) the distribution of the locally-variable value of surface electric resistance. The nature of the changes is identical for both oxidation modes, yet R_a parameter reaches relatively low values after potentiodynamic polarization to 1.9 V. This results indicate that potentiodynamic polarization leads to more uniform oxidation level.

The electrochemically active surface area plays a critical role with regard to the rate and mechanism of heterogeneous electrochemical reactions. The aforementioned assumption has been confirmed by many studies in the field of chemical engineering [71] and chemical sensing [72]. However, besides the obvious and often included geometric factor, one should also consider the non-homogeneity of electrical conductance in the electrode material. Such systems, classified as partially blocked electrodes (PBS), porous electrodes, and modified electrodes [30,70], have been studied for a long time. In certain cases, the research subject is the process of non-homogeneous adsorption, which involves the surface modification.

Subsequently, the changes in the size of kinetic and diffusion currents occur [71]. As a result, this may lead to the erroneous interpretation of data due to inadequate electrochemical scenario in relation to the classical model of electrolyte/electrode interaction [70].

The problem was investigated by Compton et al. [31,73] for highly-oriented pyrolytic graphite electrodes modified with gold nanoparticles using an approach based on defining the surface geometry by including the spatial distribution of areas characterized by different conductivity. Contrary to the situation of clear separation between conducting and isolating areas, HOPG as well as BDD electrodes display areas of heterogeneous conductance, described as electrochemically heterogeneous electrodes (EHE) [31,70].

The following situation requires the inclusion of the spatial variability of the parameters derived from the Butler-Volmer equation. Thus, the assumption has to be made that the electrochemical activity occurs on the entire surface of the electrode, although its value may differ by a couple orders of magnitude depending on location. The real existence of the above situation in relation to BDD has been proven by the changes in charge transfer resistance, as monitored *in situ* via electrochemical microscopy, as well as the occurrence of analogical changes in electrical resistance demonstrated by means of AFM [54].

The electrochemical response of redox processes occurring on the BDD surface is determined by the charge exchange kinetics. Therefore, the voltammetry analysis cannot be properly performed by applying the Randles-Sevcik model, which refers to the diffusion-controlled processes. Additionally, the effects associated with the highly inhomogeneous surface distribution of electric properties may be involved. These properties translate into the surface-dependent rate of charge exchange and, as a result, require the use of an apparent constant of the reaction rate that has been averaged [54]. Thus, it is important to analyze to what extent the nanoscale heterogeneity of EASA influences the voltammetry results.

An attempt was made to demonstrate the variability of the kinetic characteristics of the charge exchange process in dependence on the various treatment procedures. Our observations showed that this process is often unique, and the BDD electrodes prepared the same way can be characterized by a completely different electrochemical response. In Fig. 6, the voltammetry results obtained for the electrochemically oxidized BDD electrodes are shown.

Fig. 6a presents results of voltammetry analysis for unmodified BDD electrode in presence of $[Fe(CN_6)]^{3-/4-}$ redox couple. Separation between anodic and cathodic peaks increases from 108 to approx. 500 mV for applied scan rates. This variability in the *dE/dt* function indicates the irreversibility/quasi-reversibility of investigated process, which requires the use of dedicated chronovoltammetric relations. Large peak separation excludes the applicability of the Randles-Sevcik equation. Thus, an approach developed by Nicholson [74] was used. The Nicholson method allowed for the empirical determination of the standard rate constant k_0, which can be regarded as an indirect measure of the electrochemical activity on the electrode surface. It should be noted that size of peak separation is located in the boundary,

flattened part of the empirical characteristic used to estimate the standard rate constant in Nicholson method, thus the obtained value should be considered as a rough estimate. The value of $k_0 = 6.13 \cdot 10^{-3}$ cm/s indicates a relatively low charge exchange rate and significant contribution of activation control.

The linear relationship between peak currents i_p and square root of the scan rate v should be maintained for both: purely activation and diffusion control case studies. In the case of electrochemical pre-treatment by means of potentiostatic polarization performed for 20 min at 1.6 V (Fig. 6b, inset) and 2.5 V (Fig. 6c, inset), small deviations from the linearity were observed. The k_0 values of these BDD samples correspond to decrease of the reaction rate constant, to 5.7 and $4.2 \cdot 10^{-3}$ cm/s, respectively. Both of these values correspond to quasi-reversibility regime ($0.1 < k_0 < 1 \cdot 10^{-5}$ cm/s) [75]. One can notice a clear deviation from the linear course of $di_p/dv^{1/2}$ function, however the main justification for the observed anomaly appears to be the control of the electrode process rather than geometric factor. According to m-NIM and SECM studies heterogeneity of potentiostatically polarized samples fall into range of heavily overlapping diffusion layers, having smaller influence on the voltammetry results [73].

A different situation is observed in the case of surface pre-treatment in the form of potentiodynamic polarization, where the polarization procedure was carried out at a scan rate of 20 mV/s up to polarization potential of 1.6 V (Fig. 6d) and 1.9 V (Fig. 6e). According to recent studies by Ensch et al. [76] as well as own observations, the potentiodynamic polarization allows to achieve greater change in surface properties due to oxidation of termination bonds. Polarization carried out to the first of aforementioned potential values (Fig. 6d) results in appearance of strongly deformed anodic and cathodic peaks, with strong asymmetry indicating a change in process kinetics. The following case corresponds to irreversibility of investigated process, confirmed by disappearance of the cathodic peak. The relationship $di_p/dv^{1/2}$ should remain linear in the case of irreversible reaction, which is not the case when analyzing the impact of potentiodynamic polarization exceeding 1.6 V where local heterogeneity may be explain observed behavior. In the case presented on Fig. 6e the modification of electrode surface is highly homogeneous. Oxidized termination bonds covers over 99% of BDD surface, with only few small and spread areas owing high conductivity as a result (refer to Fig. 1e). Such situation may indicate that the diffusion fields of areas owing higher charge transfer rate are not overlapping each other leading to true electrochemical heterogeneity. Standard rate constant for BDD sample after potentiodynamic pre-treatment at 1.6 V was equal to $3.1 \cdot 10^{-3}$ cm/s, which is lower than any result obtained as a result of potentiostatic pre-treatment. On the other hand, k_0 is unmeasurable using Nicholson's approach due to cathodic process blockage.

The departure from linearity, due to geometric variation, in the relationship between the peak current and the square root of scan rate is dependent on many factors including the shape of individual grains as well as the rate of concentration variation per electrolyte volume [54]. Performed voltammetry analysis evidences the existence of changes in BDD structure, which translates into a different charge exchange

kinetics in the redox system under study. However, a direct connection between voltammetry plots and changes in EASA properties will be possible after numerical simulation of the current response, an approach being currently under development.

4. Summary and conclusions

We investigated the effect of the modification of boron-doped diamond electrodes via electrochemical oxidation, with the aim to elaborate how various approaches to electrochemical surface oxidation affect heterogeneous distribution of electric properties and the electrode electrochemical response. Both studied pre-treatment types led to the oxidation of terminal functional groups to the hydroxyl, and to some extent, carboxyl and carbonyl species. The direct effect of the oxidation process was the increase in electric surface resistance but also the charge transfer resistance. More importantly, the modification process was gradual and dependent on the polarization voltage. The m-NIM studies revealed local heterogeneous distribution of surface resistance across the BDD electrode, which is associated with its crystallographic structure. The highest level of heterogeneity was observed during potentiostatic polarization in BDD electrodes exposed to moderate polarization voltages, reaching 1.6 V vs Ag|AgCl.

The SECM, DEIS and CV studies were carried out to demonstrate how the heterogeneous distribution of electric resistance affects BDD response under electrolytic conditions. DEIS allowed to monitor the oxidation process, which resulted in the conclusion that the sample homogeneity decreases for the polarization voltage equal to or exceeding 1.6 V vs Ag|AgCl. The observed heterogeneity of electrochemical activity proved to be in agreement with the results of m-NIM studies. The voltammetry studies revealed significant deviations determined by both the numerical analysis and experimental observations, which casts doubt on the correctness of data interpretation in relation to the behavior of heterogeneous electrodes assessed by classical voltammetry approach.

Most importantly, it was proven that even small differences in electrochemical pre-treatment conditions has the key role on the BDD electrode response and thus on its possible application. Since polycrystalline BDD electrodes are characterized by high and uncontrolled level of surface heterogeneity, detailed and precise description of the pre-treatment process must be given every time.

Acknowledgements:

The authors gratefully acknowledge financial support from the National Science Centre under projects Sonata No. 2015/17/ST5/02571, Preludium No. 2015/19/N/ST5/02659 and National Centre for Science and Development project Techmatstrateg No. 347324. The DS funds of the Faculty of Chemistry and Faculty of Electronics, Telecommunications and Informatics of the Gdansk University of Technology are also acknowledged.

Figures:

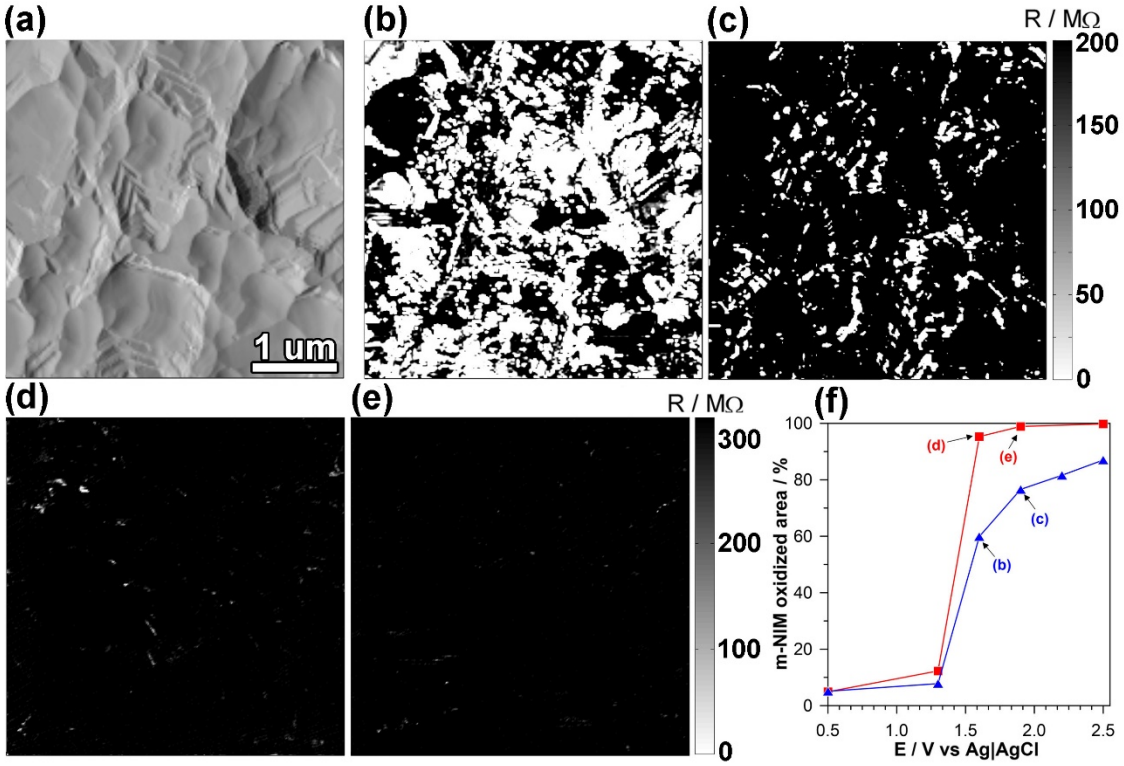

Fig. 1 – (a) AFM contour micrograph and (b-e) m-NIM maps presenting the parallel (surface) resistance distribution for a BDD sample after various electrochemical pre-treatments: potentiostatic polarization (b) at 1.6 and (c) 2.5 V; potentiodynamic polarization (d) up to 1.6 and (e) up to 1.9 V. Reference electrode Ag|AgCl. (f) evolution of oxidized BDD surface area under applied conditions, based on the m-NIM studies.

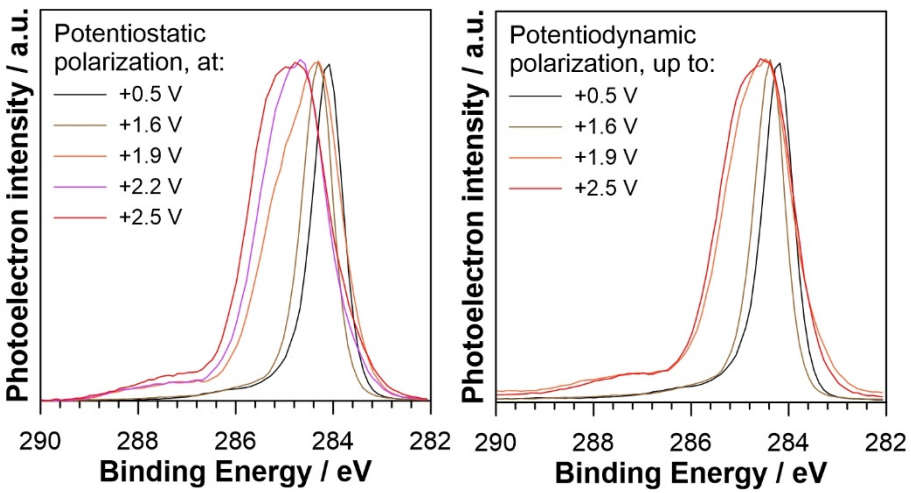

Fig. 2 - High-resolution XPS spectra in the *C1s* energy range for BDD electrodes subjected to the potentiostatic and potentiodynamic polarization pre-treatments at various conditions.

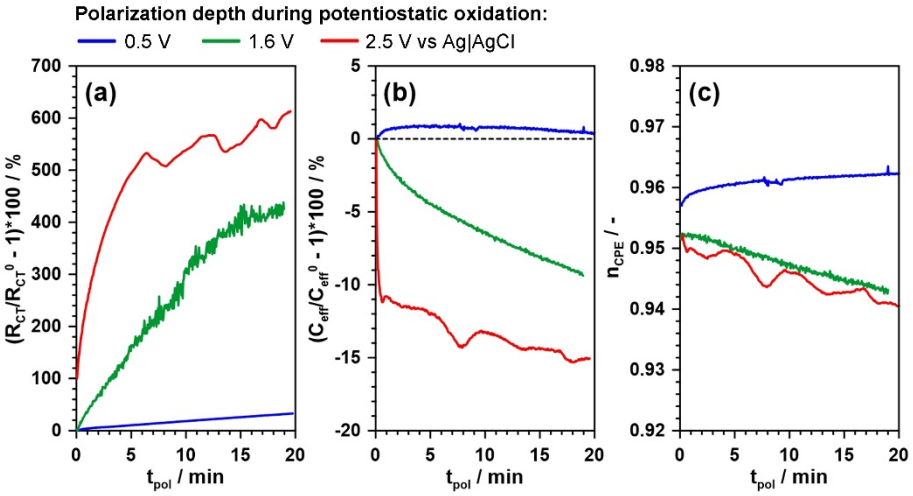

Fig. 3 – The results of dynamic impedance monitoring via DEIS recorded during the potentiostatic oxidation experiment at various anodic polarization depths: 0.5 V vs Ag|AgCl (blue line), 1.6 V (green), 2.5 V (red). Relative changes of (a) charge transfer resistance R_{CT}, (b) effective capacitance calculated on the basis of the surface distribution model, and (c) changes in the CPE exponent n. Impedance data were fitted using R(QR) electric equivalent circuit.

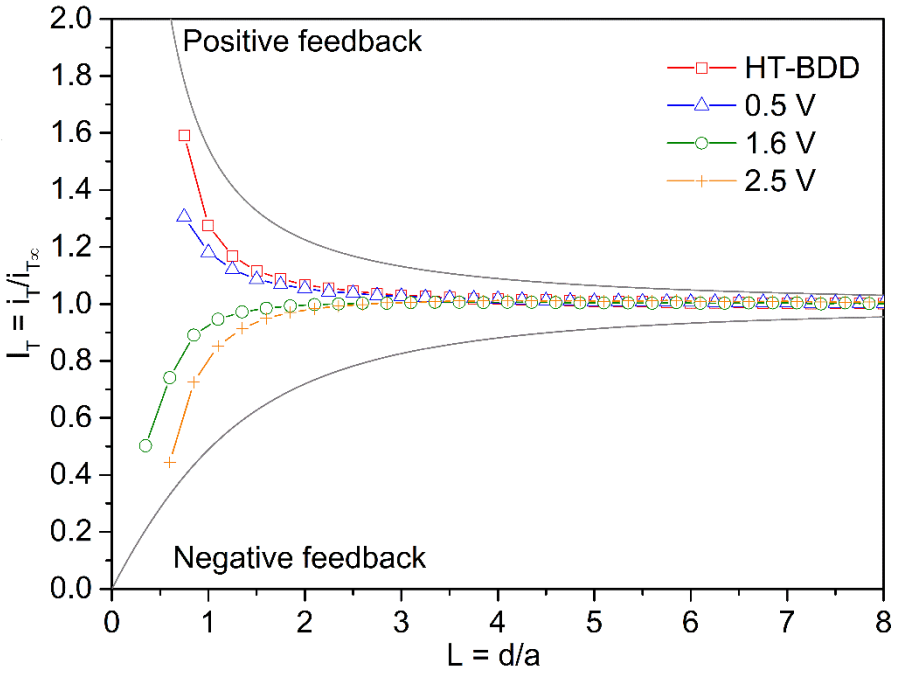

Fig. 4 – SECM approach curves for BDD electrodes oxidized electrochemically. *L* normalized distance, *d* distance of UME to the specimen surface, *a* is a diameter of platinum disk in an insulating sheath, I_T is a normalized current, i_T current at the UME tip, and $i_{T\infty}$ is a tip current in the bulk.

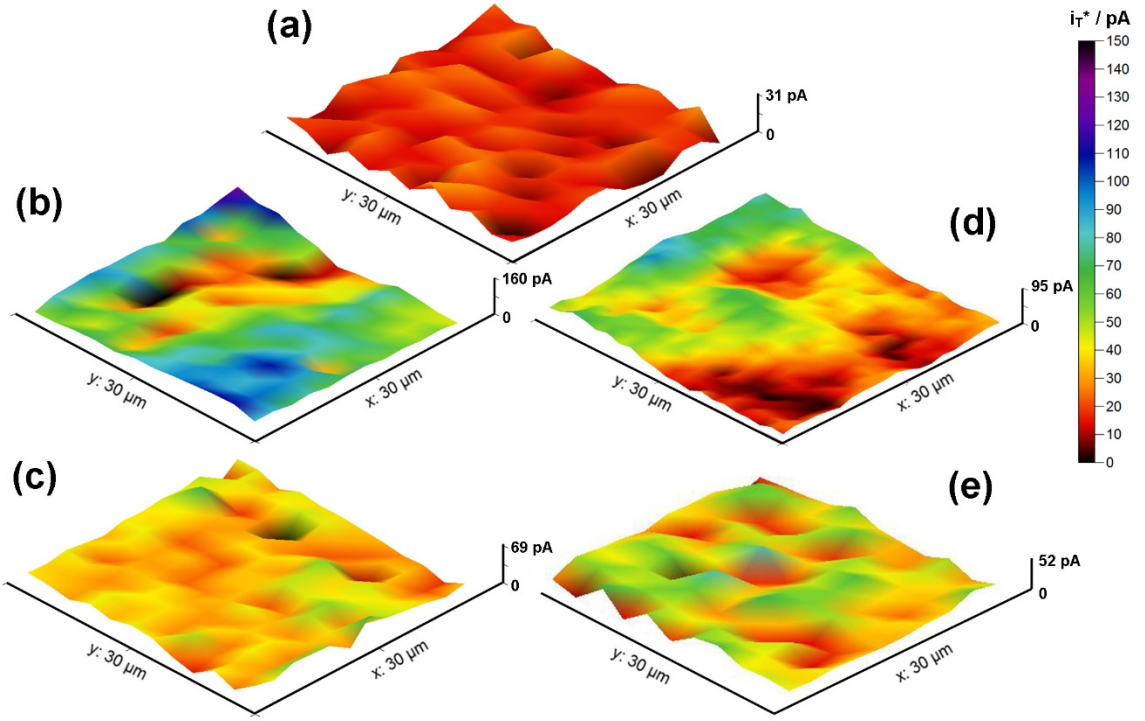

Fig. 5 – Scanning electrochemical microscopy (SECM) micrographs recorded after electrochemical oxidation pre-treatment, which was potentiostatic polarization at: (a) 0.5 V, (b) 1.6 V, (c) 2.5 V or potentiodynamic polarization up to: (d) 1.6 V, (e) 1.9 V. Reference electrode: Ag|AgCl.

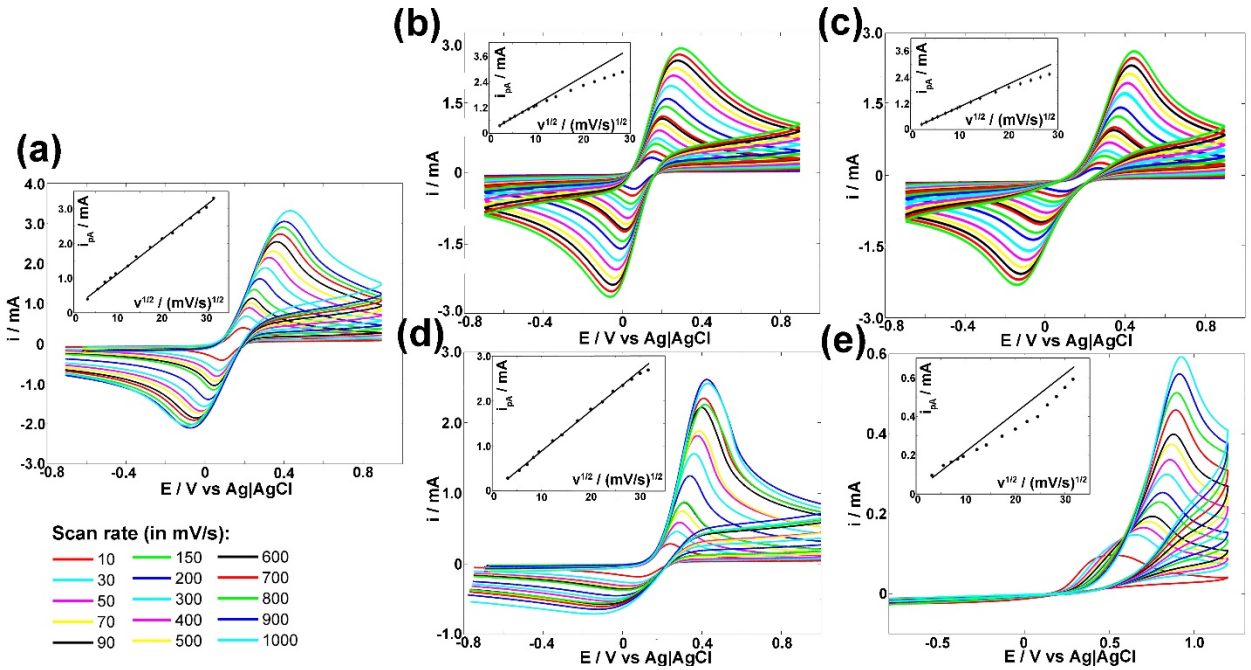

Fig. 6 – Chronovoltammograms carried out for (a) reference sample; after potentiostatic polarization at: (b) 1.6 V and (c) 2.5 V; after potentiodynamic polarization to: (d) 1.6 V and (e) 1.9 V. Reference electrode Ag|AgCl. In the inset resultant $i_p = f(v^{1/2})$ slopes representing the Randles-Sevcik relationship for each BDD sample.

Table 1 - Surface chemical composition after anodic polarization of BDD electrodes in potentiostatic mode, based on high-resolution XPS analysis in the *C1s* BE range.

		$C\text{-}C_H$	$C\text{-}C_O$	C-OH	C=O	sp^2-C
		284.2 eV	285.0 eV	285.9 eV	287.3*eV	283.2 eV
Potentiostatic polarization	at 0.5 V	86.2	7.7	4.2	1.7	0.2
	at 1.6 V	88.1	6.8	3.0	1.7	0.4
	at 1.9 V	50.8	38.2	3.7	5.6	1.7
	at 2.5 V	37.3	43.4	9.4	6.9	3.0
Potentiodynamic polarization	to 1.6 V	73.8	15.5	6.6	2.3	1.8
	to 1.9 V	41.5	42.2	7.7	5.2	3.4
	to 2.5 V	41.3	36.5	13.5	5.6	3.1

* The share of carbon marked as C=O is a sum of two peaks, located at 287.0 eV for carbonyl and 288.8 eV for carboxyl species.

Table 2 – The values of initial charge transfer resistance, R_{CT}^0 and effective capacitance, C_{eff}^0 recorded for BDD samples during the first 30 seconds of potentiostatic polarization experiment at various polarization potentials.

Polarization depth	R_{CT} / kΩ	C_{eff} / μF
0.5 V	51.20	0.91
1.6 V	0.70	1.19
2.5 V	0.023	1.38

Table 3 – Arithmetic mean deviation R_a of EASA profiles measured via SECM, in pA.

Polarization / V vs Ag|AgCl	0.5	1.6	1.9	2.5
Potentiostatic polarization	4.4	18.4	13.2	7.6
Potentiodynamic polarization	4.0	15.6	7.7	5.1

References:

[1] T.A. Ivandini, Y. Einaga, Polycrystalline boron-doped diamond electrodes for electrocatalytic and electrosynthetic applications, Chem. Commun. 53 (2017) 1338–1347. doi:10.1039/C6CC08681K.

[2] Z.J. Ayres, J.C. Newland, M.E. Newton, S. Mandal, O.A. Williams, J.V. Macpherson, Impact of chemical vapour deposition plasma inhomogeneity on the spatial variation of sp2 carbon in boron doped diamond electrodes, Carbon. 121 (2017) 434–442. doi:10.1016/j.carbon.2017.06.008.

[3] S.J. Cobb, Z.J. Ayres, J.V. Macpherson, Boron Doped Diamond: A Designer Electrode Material for the Twenty-First Century, Annu. Rev. Anal. Chem. 11 (2018) 463–484. doi:10.1146/annurev-anchem-061417-010107.

[4] T. Watanabe, S. Yoshioka, T. Yamamoto, H. Sepehri-Amin, T. Ohkubo, S. Matsumura, Y. Einaga, The local structure in heavily boron-doped diamond and the effect this has on its electrochemical properties, Carbon. 137 (2018) 333–342. doi:10.1016/j.carbon.2018.05.026.

[5] L.A. Hutton, J.G. Iacobini, E. Bitziou, R.B. Channon, M.E. Newton, J.V. Macpherson, Examination of the Factors Affecting the Electrochemical Performance of Oxygen-Terminated Polycrystalline Boron-Doped Diamond Electrodes, Anal. Chem. 85 (2013) 7230–7240. doi:10.1021/ac401042t.

[6] J.V. Macpherson, A practical guide to using boron doped diamond in electrochemical research, Phys. Chem. Chem. Phys. 17 (2015) 2935–2949. doi:10.1039/C4CP04022H.

[7] J.A. Bennett, J. Wang, Y. Show, G.M. Swain, Effect of sp2-Bonded Nondiamond Carbon Impurity on the Response of Boron-Doped Polycrystalline Diamond Thin-Film Electrodes, J. Electrochem. Soc. 151 (2004) E306–E313. doi:10.1149/1.1780111.

[8] J. Ryl, L. Burczyk, R. Bogdanowicz, M. Sobaszek, K. Darowicki, Study on surface termination of boron-doped diamond electrodes under anodic polarization in H 2 SO 4 by means of dynamic impedance technique, Carbon. 96 (2016) 1093–1105. doi:10.1016/j.carbon.2015.10.064.

[9] M. Tachiki, T. Fukuda, K. Sugata, H. Seo, H. Umezawa, H. Kawarada, Nanofabrication on Hydrogen-Terminated Diamond Surfaces by Atomic Force Microscope Probe-Induced Oxidation, Jpn. J. Appl. Phys. 39 (2000) 4631–4632. doi:10.1143/JJAP.39.4631.

[10] I. Yagi, H. Notsu, T. Kondo, D.A. Tryk, A. Fujishima, Electrochemical selectivity for redox systems at oxygen-terminated diamond electrodes, J. Electroanal. Chem. 473 (1999) 173–178. doi:10.1016/S0022-0728(99)00027-3.

[11] K. Hayashi, S. Yamanaka, H. Watanabe, T. Sekiguchi, H. Okushi, K. Kajimura, Investigation of the effect of hydrogen on electrical and optical properties in chemical vapor deposited on homoepitaxial diamond films, J. Appl. Phys. 81 (1997) 744–753. doi:10.1063/1.364299.

[12] H.A. Girard, E. de La Rochefoucauld, D. Ballutaud, A. Etcheberry, N. Simon, Controlled Anodic Treatments on Boron-Doped Diamond Electrodes Monitored by Contact Angle Measurements, Electrochem. Solid-State Lett. 10 (2007) F34–F37. doi:10.1149/1.2743824.

[13] N. Simon, H. Girard, D. Ballutaud, S. Ghodbane, A. Deneuville, M. Herlem, A. Etcheberry, Effect of H and O termination on the charge transfer of moderately boron doped diamond electrodes, Diam. Relat. Mater. 14 (2005) 1179–1182. doi:10.1016/j.diamond.2004.12.013.

[14] H. Girard, N. Simon, D. Ballutaud, M. Herlem, A. Etcheberry, Effect of anodic and cathodic treatments on the charge transfer of boron doped diamond electrodes, Diam. Relat. Mater. 16 (2007) 316–325. doi:10.1016/j.diamond.2006.06.009.

[15] S.C. B. Oliveira, A.M. Oliveira-Brett, Voltammetric and electrochemical impedance spectroscopy characterization of a cathodic and anodic pre-treated boron doped diamond electrode, Electrochimica Acta. 55 (2010) 4599–4605. doi:10.1016/j.electacta.2010.03.016.

[16] B.P. Chaplin, D.K. Hubler, J. Farrell, Understanding anodic wear at boron doped diamond film electrodes, Electrochimica Acta. 89 (2013) 122–131. doi:10.1016/j.electacta.2012.10.166.

[17] R. Trouillon, Y. Einaga, M.A.M. Gijs, Cathodic pretreatment improves the resistance of boron-doped diamond electrodes to dopamine fouling, Electrochem. Commun. 47 (2014) 92–95. doi:10.1016/j.elecom.2014.07.028.

[18] M. Wang, N. Simon, C. Decorse-Pascanut, M. Bouttemy, A. Etcheberry, M. Li, R. Boukherroub, S. Szunerits, Comparison of the chemical composition of boron-doped diamond surfaces upon different oxidation processes, Electrochimica Acta. 54 (2009) 5818–5824. doi:10.1016/j.electacta.2009.05.037.

[19] Y.V. Pleskov, Y.E. Evstefeeva, M.D. Krotova, V.P. Varnin, I.G. Teremetskaya, Synthetic semiconductor diamond electrodes: Electrochemical behaviour of homoepitaxial boron-doped films orientated as (111), (110), and (100) faces, J. Electroanal. Chem. 595 (2006) 168–174. doi:10.1016/j.jelechem.2006.07.010.

[20] R. Hoffmann, H. Obloh, N. Tokuda, N. Yang, C.E. Nebel, Fractional Surface Termination of Diamond by Electrochemical Oxidation, Langmuir. 28 (2012) 47–50. doi:10.1021/la2039366.

[21] N.R. Wilson, S.L. Clewes, M.E. Newton, P.R. Unwin, J.V. Macpherson, Impact of Grain-Dependent Boron Uptake on the Electrochemical and Electrical Properties of Polycrystalline Boron Doped Diamond Electrodes, J. Phys. Chem. B. 110 (2006) 5639–5646. doi:10.1021/jp0547616.
[22] Y.V. Pleskov, Y.E. Evstefeeva, V.P. Varnin, I.G. Teremetskaya, Synthetic Semiconductor Diamond Electrodes: Electrochemical Characteristics of Homoepitaxial Boron-doped Films Grown at the (111), (110), and (100) Faces of Diamond Crystals, Russ. J. Electrochem. 40 (2004) 886–892. doi:10.1023/B:RUEL.0000041354.70107.c8.
[23] J. Ryl, R. Bogdanowicz, P. Slepski, M. Sobaszek, K. Darowicki, Dynamic Electrochemical Impedance Spectroscopy (DEIS) as a Tool for Analyzing Surface Oxidation Processes on Boron-Doped Diamond Electrodes, J. Electrochem. Soc. 161 (2014) H359–H364. doi:10.1149/2.016406jes.
[24] S. Ghodbane, D. Ballutaud, F. Omnès, C. Agnès, Comparison of the XPS spectra from homoepitaxial {111}, {100} and polycrystalline boron-doped diamond films, Diam. Relat. Mater. 19 (2010) 630–636. doi:10.1016/j.diamond.2010.01.014.
[25] A. Zieliński, R. Bogdanowicz, J. Ryl, L. Burczyk, K. Darowicki, Local impedance imaging of boron-doped polycrystalline diamond thin films, Appl. Phys. Lett. 105 (2014) 131908. doi:10.1063/1.4897346.
[26] J. Ryl, A. Zielinski, L. Burczyk, R. Bogdanowicz, T. Ossowski, K. Darowicki, Chemical-Assisted Mechanical Lapping of Thin Boron-Doped Diamond Films: A Fast Route Toward High Electrochemical Performance for Sensing Devices, Electrochimica Acta. 242 (2017) 268–279. doi:10.1016/j.electacta.2017.05.027.
[27] J. Ryl, A. Zielinski, R. Bogdanowicz, K. Darowicki, Heterogeneous distribution of surface electrochemical activity in polycrystalline highly boron-doped diamond electrodes under deep anodic polarization, Electrochem. Commun. 83 (2017) 41–45. doi:10.1016/j.elecom.2017.08.019.
[28] A. Zielinski, M. Cieslik, M. Sobaszek, R. Bogdanowicz, K. Darowicki, J. Ryl, Multifrequency Nanoscale Impedance Microscopy (m-NIM): A novel approach towards detection of selective and subtle modifications on the surface of polycrystalline boron-doped diamond electrodes, Preprint. (2018). doi:https://arxiv.org/abs/1811.05709.
[29] R. Hoffmann, A. Kriele, H. Obloh, N. Tokuda, W. Smirnov, N. Yang, C.E. Nebel, The creation of a biomimetic interface between boron-doped diamond and immobilized proteins, Biomaterials. 32 (2011) 7325–7332. doi:10.1016/j.biomaterials.2011.06.052.
[30] B.A. Brookes, T.J. Davies, A.C. Fisher, R.G. Evans, S.J. Wilkins, K. Yunus, J.D. Wadhawan, R.G. Compton, Computational and Experimental Study of the Cyclic Voltammetry Response of Partially Blocked Electrodes. Part 1. Nonoverlapping, Uniformly Distributed Blocking Systems, J. Phys. Chem. B. 107 (2003) 1616–1627. doi:10.1021/jp021810v.
[31] T.J. Davies, R.R. Moore, C.E. Banks, R.G. Compton, The cyclic voltammetric response of electrochemically heterogeneous surfaces, J. Electroanal. Chem. 574 (2004) 123–152. doi:10.1016/j.jelechem.2004.07.031.
[32] R. Bogdanowicz, M. Sawczak, P. Niedzialkowski, P. Zieba, B. Finke, J. Ryl, J. Karczewski, T. Ossowski, Novel Functionalization of Boron-Doped Diamond by Microwave Pulsed-Plasma Polymerized Allylamine Film, J. Phys. Chem. C. 118 (2014) 8014–8025. doi:10.1021/jp5003947.
[33] M. Ficek, M. Sobaszek, M. Gnyba, J. Ryl, ł. Gołuński, M. Smietana, J. Jasiński, P. Caban, R. Bogdanowicz, Optical and electrical properties of boron doped diamond thin conductive films deposited on fused silica glass substrates, Appl. Surf. Sci. 387 (2016) 846–856. doi:10.1016/j.apsusc.2016.06.165.
[34] K. Siuzdak, R. Bogdanowicz, M. Sawczak, M. Sobaszek, Enhanced capacitance of composite TiO_2 nanotube/boron-doped diamond electrodes studied by impedance spectroscopy, Nanoscale. 7 (2015) 551–558. doi:10.1039/C4NR04417G.
[35] D. Nidzworski, K. Siuzdak, P. Niedziałkowski, R. Bogdanowicz, M. Sobaszek, J. Ryl, P. Weiher, M. Sawczak, E. Wnuk, W.A. Goddard, A. Jaramillo-Botero, T. Ossowski, A rapid-response ultrasensitive biosensor for influenza virus detection using antibody modified boron-doped diamond, Sci. Rep. 7 (2017) 15707. doi:10.1038/s41598-017-15806-7.
[36] A. Zieliński, K. Darowicki, Application of multisine nanoscale impedance microscopy to heterogeneous alloy surface investigations: Application of multisine NIM to alloy surface investigations, Surf. Interface Anal. 47 (2015) 1109–1113. doi:10.1002/sia.5855.
[37] K. Darowicki, Theoretical description of the measuring method of instantaneous impedance spectra, J. Electroanal. Chem. 486 (2000) 101–105. doi:10.1016/S0022-0728(00)00110-8.
[38] P. Slepski, K. Darowicki, E. Janicka, G. Lentka, A complete impedance analysis of electrochemical cells used as energy sources, J. Solid State Electrochem. 16 (2012) 3539–3549. doi:10.1007/s10008-012-1825-1.
[39] K. Darowicki, P. Ślepski, Dynamic electrochemical impedance spectroscopy of the first order electrode reaction, J. Electroanal. Chem. 547 (2003) 1–8. doi:10.1016/S0022-0728(03)00154-2.

[40] G.A. Ragoisha, A.S. Bondarenko, Potentiodynamic Electrochemical Impedance Spectroscopy for Solid State Chemistry, Solid State Phenom. 90–91 (2003) 103–108. doi:10.4028/www.scientific.net/SSP.90-91.103.
[41] H. Gerengi, H. Goksu, P. Slepski, The inhibition effect of mad Honey on corrosion of 2007-type aluminium alloy in 3.5% NaCl solution, Mater. Res. 17 (2014) 255–264. doi:10.1590/S1516-14392013005000174.
[42] J. Ryl, K. Darowicki, Impedance Monitoring of Carbon Steel Cavitation Erosion under the Influence of Corrosive Factors, J. Electrochem. Soc. 155 (2008) P44–P49. doi:10.1149/1.2840619.
[43] M.A. Amin, N. El-Bagoury, M.H.H. Mahmoud, M.M. Hessien, S.S. Abd El-Rehim, J. Wysocka, J. Ryl, Catalytic impact of alloyed Al on the corrosion behavior of $Co_{50} Ni_{23} Ga_{26} Al_{1.0}$ magnetic shape memory alloy and catalysis applications for efficient electrochemical H_2 generation, RSC Adv. 7 (2017) 3635–3649. doi:10.1039/C6RA25384A.
[44] H. Gerengi, P. Slepski, E. Ozgan, M. Kurtay, Investigation of corrosion behavior of 6060 and 6082 aluminum alloys under simulated acid rain conditions: Corrosion behavior of 6060 and 6082 Al alloys under acid rain, Mater. Corros. 66 (2015) 233–240. doi:10.1002/maco.201307287.
[45] M. Szociński, K. Darowicki, K. Schaefer, Application of impedance imaging to evaluation of organic coating degradation at a local scale, J. Coat. Technol. Res. 10 (2013) 65–72. doi:10.1007/s11998-012-9458-y.
[46] B. Wouters, R. Claessens, A. Hubin, H. Terryn, On the use of instantaneous impedance for post-electrochemical treatment analysis, Electrochem. Commun. 93 (2018) 187–190. doi:10.1016/j.elecom.2018.07.014.
[47] K. Darowicki, S. Krakowiak, P. Slepski, The time dependence of pit creation impedance spectra, Electrochem. Commun. 6 (2004) 860–866. doi:10.1016/j.elecom.2004.06.010.
[48] L. Burczyk, K. Darowicki, Local electrochemical impedance spectroscopy in dynamic mode of galvanic coupling, Electrochimica Acta. 282 (2018) 304–310. doi:10.1016/j.electacta.2018.05.192.
[49] J. Wysocka, S. Krakowiak, J. Ryl, Evaluation of citric acid corrosion inhibition efficiency and passivation kinetics for aluminium alloys in alkaline media by means of dynamic impedance monitoring, Electrochimica Acta. 258 (2017) 1463–1475. doi:10.1016/j.electacta.2017.12.017.
[50] J. Orlikowski, J. Ryl, M. Jarzynka, S. Krakowiak, K. Darowicki, Instantaneous Impedance Monitoring of Aluminum Alloy 7075 Corrosion in Borate Buffer with Admixed Chloride Ions, CORROSION. 71 (2015) 828–838. doi:10.5006/1546.
[51] A.S. Bondarenko, I.E.L. Stephens, H.A. Hansen, F.J. Pérez-Alonso, V. Tripkovic, T.P. Johansson, J. Rossmeisl, J.K. Nørskov, I. Chorkendorff, The Pt(111)/Electrolyte Interface under Oxygen Reduction Reaction Conditions: An Electrochemical Impedance Spectroscopy Study, Langmuir. 27 (2011) 2058–2066. doi:10.1021/la1042475.
[52] R. O'Hayre, G. Feng, W.D. Nix, F.B. Prinz, Quantitative impedance measurement using atomic force microscopy, J. Appl. Phys. 96 (2004) 3540–3549. doi:10.1063/1.1778217.
[53] F. Gao, L. Han, Implementing the Nelder-Mead simplex algorithm with adaptive parameters, Comput. Optim. Appl. 51 (2012) 259–277. doi:10.1007/s10589-010-9329-3.
[54] K.B. Holt, A.J. Bard, Y. Show, G.M. Swain, Scanning Electrochemical Microscopy and Conductive Probe Atomic Force Microscopy Studies of Hydrogen-Terminated Boron-Doped Diamond Electrodes with Different Doping Levels, J. Phys. Chem. B. 108 (2004) 15117–15127. doi:10.1021/jp048222x.
[55] C. Deslouis, J. de Sanoit, S. Saada, C. Mer, A. Pailleret, H. Cachet, P. Bergonzo, Electrochemical behaviour of (111) B-Doped Polycrystalline Diamond: Morphology/surface conductivity/activity assessed by EIS and CS-AFM, Diam. Relat. Mater. 20 (2011) 1–10. doi:10.1016/j.diamond.2010.10.005.
[56] R. Bogdanowicz, Characterization of Optical and Electrical Properties of Transparent Conductive Boron-Doped Diamond thin Films Grown on Fused Silica, Metrol. Meas. Syst. 21 (2014) 381–388. doi:10.2478/mms-2014-0059.
[57] Z.L. Wang, C. Lu, J.J. Li, C.Z. Gu, Effect of gas composition on the growth and electrical properties of boron-doped diamond films, Diam. Relat. Mater. 18 (2009) 132–135. doi:10.1016/j.diamond.2008.10.040.
[58] P. Niedziałkowski, R. Bogdanowicz, P. Zięba, J. Wysocka, J. Ryl, M. Sobaszek, T. Ossowski, Melamine-modified Boron-doped Diamond towards Enhanced Detection of Adenine, Guanine and Caffeine, Electroanalysis. 28 (2016) 211–221. doi:10.1002/elan.201500528.
[59] M. Wang, N. Simon, G. Charrier, M. Bouttemy, A. Etcheberry, M. Li, R. Boukherroub, S. Szunerits, Distinction between surface hydroxyl and ether groups on boron-doped diamond electrodes using a chemical approach, Electrochem. Commun. 12 (2010) 351–354. doi:10.1016/j.elecom.2009.12.029.
[60] H.A. Girard, N. Simon, D. Ballutaud, A. Etcheberry, Correlation between flat-band potential position and oxygenated termination nature on boron-doped diamond electrodes, Comptes Rendus Chim. 11 (2008) 1010–1015. doi:10.1016/j.crci.2008.01.014.
[61] R. Trouillon, D. O'Hare, Comparison of glassy carbon and boron doped diamond electrodes: Resistance to biofouling, Electrochimica Acta. 55 (2010) 6586–6595. doi:10.1016/j.electacta.2010.06.016.

[62] J. Hernando, S.Q. Lud, P. Bruno, D.M. Gruen, M. Stutzmann, J.A. Garrido, Electrochemical impedance spectroscopy of oxidized and hydrogen-terminated nitrogen-induced conductive ultrananocrystalline diamond, Electrochimica Acta. 54 (2009) 1909–1915. doi:10.1016/j.electacta.2008.10.041.
[63] S. Garcia-Segura, E. Vieira dos Santos, C.A. Martínez-Huitle, Role of sp3/sp2 ratio on the electrocatalytic properties of boron-doped diamond electrodes: A mini review, Electrochem. Commun. 59 (2015) 52–55. doi:10.1016/j.elecom.2015.07.002.
[64] Y.A. Mankelevich, P.W. May, New insights into the mechanism of CVD diamond growth: Single crystal diamond in MW PECVD reactors, Diam. Relat. Mater. 17 (2008) 1021–1028. doi:10.1016/j.diamond.2008.03.022.
[65] A. Denisenko, C. Pietzka, A. Romanyuk, H. El-Hajj, E. Kohn, The electronic surface barrier of boron-doped diamond by anodic oxidation, J. Appl. Phys. 103 (2008) 014904. doi:10.1063/1.2827481.
[66] H. Notsu, Introduction of Oxygen-Containing Functional Groups onto Diamond Electrode Surfaces by Oxygen Plasma and Anodic Polarization, Electrochem. Solid-State Lett. 2 (1999) 522. doi:10.1149/1.1390890.
[67] B. Hirschorn, M.E. Orazem, B. Tribollet, V. Vivier, I. Frateur, M. Musiani, Determination of effective capacitance and film thickness from constant-phase-element parameters, Electrochimica Acta. 55 (2010) 6218–6227. doi:10.1016/j.electacta.2009.10.065.
[68] P.R. Unwin, A.J. Bard, Scanning electrochemical microscopy. 9. Theory and application of the feedback mode to the measurement of following chemical reaction rates in electrode processes, J. Phys. Chem. 95 (1991) 7814–7824. doi:10.1021/j100173a049.
[69] A.J. Bard, M.V. Mirkin, P.R. Unwin, D.O. Wipf, Scanning electrochemical microscopy. 12. Theory and experiment of the feedback mode with finite heterogeneous electron-transfer kinetics and arbitrary substrate size, J. Phys. Chem. 96 (1992) 1861–1868. doi:10.1021/j100183a064.
[70] T.J. Davies, C.E. Banks, R.G. Compton, Voltammetry at spatially heterogeneous electrodes, J. Solid State Electrochem. 9 (2005) 797–808. doi:10.1007/s10008-005-0699-x.
[71] J. Zhao, A. Ozden, S. Shahgaldi, I.E. Alaefour, X. Li, F. Hamdullahpur, Effect of Pt loading and catalyst type on the pore structure of porous electrodes in polymer electrolyte membrane (PEM) fuel cells, Energy. 150 (2018) 69–76. doi:10.1016/j.energy.2018.02.134.
[72] F. Schröper, D. Brüggemann, Y. Mourzina, B. Wolfrum, A. Offenhäusser, D. Mayer, Analyzing the electroactive surface of gold nanopillars by electrochemical methods for electrode miniaturization, Electrochimica Acta. 53 (2008) 6265–6272. doi:10.1016/j.electacta.2008.03.068.
[73] C. Amatore, J.M. Savéant, D. Tessier, Charge transfer at partially blocked surfaces, J. Electroanal. Chem. Interfacial Electrochem. 147 (1983) 39–51. doi:10.1016/S0022-0728(83)80055-2.
[74] R.S. Nicholson, Theory and Application of Cyclic Voltammetry for Measurement of Electrode Reaction Kinetics., Anal. Chem. 37 (1965) 1351–1355. doi:10.1021/ac60230a016.
[75] J. Heinze, Cyclovoltammetrie — die „Spektroskopie" des Elektrochemikers, Angew. Chem. 96 (1984) 823–840. doi:10.1002/ange.19840961104.
[76] M. Ensch, V.Y. Maldonado, G.M. Swain, R. Rechenberg, M.F. Becker, T. Schuelke, C.A. Rusinek, Isatin Detection Using a Boron-Doped Diamond 3-in-1 Sensing Platform, Anal. Chem. 90 (2018) 1951–1958. doi:10.1021/acs.analchem.7b04045.